

Path Loss Prediction Using Deep Learning

Ryan Dempsey*[†], Jonathan Ethier*, Halim Yanikomeroglu[†]

*Communications Research Centre (CRC), Ottawa, ON, Canada: {ryan.dempsey, jonathan.ethier}@ised-isde.gc.ca

[†]Carleton University, Ottawa, ON, Canada: ryandempsey@cmail.carleton.ca, halim@sce.carleton.ca

Abstract—Radio deployments and spectrum planning can benefit from path loss predictions. Obstructions along a communications link are often considered implicitly or through derived metrics such as representative clutter height or total obstruction depth. In this paper, we propose a path-specific path loss prediction method that uses convolutional neural networks to automatically perform feature extraction from high-resolution obstruction height maps. Our methods result in low prediction error in a variety of environments without requiring derived obstruction metrics.

Index Terms—Drive test measurements, machine learning, obstructions, path loss modeling.

I. INTRODUCTION

PROPAGATION models are used by the wireless industry and regulatory bodies to aid in analysis to enhance wireless coverage and avoid unwanted interference. Path loss modeling, a common approach to propagation modeling, aims to predict point-to-point (P2P) wireless signal attenuation along the communications link from the transmitter (Tx) to the receiver (Rx). The three main factors in predicting path loss are carrier frequency, link distance, and obstructions in the line of sight (LOS). In LOS conditions, free space path loss (FSPL), which uses frequency and distance, is sufficient for accurate P2P path loss predictions. In non-LOS conditions, however, FSPL tends to severely underestimate path loss.

LOS obstructions are obtained through surface-level variations, which are captured by the geographic information system (GIS) quantity digital surface model (DSM). DSM is measured relative to sea level and captures all heights, which can include ground-level variations (terrain) as well as trees, buildings, and other structures (clutter). Where no clutter is present, DSM models the terrain.

Traditional path loss models, such as Longley-Rice [1], explicitly account for terrain information but do not explicitly consider the presence of clutter. Consequently, these predictions can underestimate path loss in links dominated by clutter.

Modern path loss models that consider clutter information have been shown to significantly decrease prediction error in non-LOS links. One such model, P.1812-6 [2] (recommended by the International Telecommunications Union Radiocommunication Sector (ITU-R)), considers clutter along the link in the form of representative clutter heights. The values of these heights are computed using local information regarding the types of clutter present. This yields more accurate predictions, but there is room for improvement due to the approximations imposed by the representative clutter height computation and the emphasis on diffraction losses [3].

Previous work in [3] shows improvement over P.1812-6 in non-LOS conditions, by capturing GIS information in one

novel feature: total obstruction depth. This scalar feature is computed using surface information along the direct path. Alongside frequency and distance, obstruction depth yields a root mean square error (RMSE) in the range of 6-8 dB [3] as compared to 8-13 dB for P.1812-6. While using total obstruction depth as a feature can produce lower errors, the feature is a single scalar value derived from the surface profile. It does not explicitly consider the surface height profile, which can influence path loss in more complicated ways due to diffraction and Fresnel zone effects [4].

The goal of this paper is to explicitly utilize the surface profile to train a path-specific propagation model. Leveraging high-resolution clutter maps and deep neural networks to directly predict path loss, we aim to study whether high-dimensional spatial features can be extracted more reliably by neural networks than by human-defined feature engineering. The secondary goal is to compare whether these complex features are improved by adding the transverse dimension (the dimension perpendicular to the link distance).

Previous work [5] uses map-based inputs to train path loss models limited to two frequencies within a single area, with no geographically distinct tests. Random cross-validation using spatial data can lead to data leakage which can lead to overfitting [6]. Our work aims to construct generalized models that can predict path loss in unseen scenarios, which can only be judged through blind testing.

This paper describes path loss models trained on one- and two-dimensional (1D & 2D) surface height data alongside measurement data. Section II describes the pre-processed datasets used to train and evaluate the path loss models. Section III justifies the multi-dimensional features used from the data and details the model architectures used for the 1D and 2D clutter height data. Section IV describes the training and evaluation process and results. Finally, Section V summarizes our findings and presents potential future directions.

II. DATA PREPARATION

A. Dataset Description

There are two types of data used in this work: radio measurement data, and geographic elevation/clutter data. For radio measurement data, we use drive test measurement data from the United Kingdom Office of Communications (UK Ofcom) [7], which can be accessed by the general public through Ofcom's open data repository [8]. This dataset was collected between 2015 and 2018, and provides 8.2 million measurements across six frequencies (449, 915, 1802, 2695, 3602, and 5850 MHz) in seven cities in the UK. Each city uses a single Tx with varying Rx locations. Link distances vary from 1 m to 78 km, with a median of 8 km.

For clutter data, we use the UK open digital elevation model (DEM) [9]. This dataset provides DSM at a 1 m resolution for various areas across the UK. DEM data is available for six out of seven drive test cities: Boston, London, Merthyr Tydfil, Nottingham, Southampton, and Stevenage. We use data from these six cities to train and test our path loss models.

The following subsection discusses the steps taken to filter, pre-process, and join these two datasets.

B. Data Cleaning

1) *Ofcom drive test data*: Firstly, we use measurements with received signal level (RSL) above the system noise floor provided in the dataset, by a 6 dB margin, as shown in (1a). We exclude measurements near and below the noise floor to ensure the model is trained on reliable data. Similarly, we use only links with a total distance d above 50 meters as in (1b):

$$RSL \text{ [dBm]} > \text{noise floor [dBm]} + 6 \text{ dB}, \quad (1a)$$

$$d \text{ [m]} > 50 \text{ m}. \quad (1b)$$

This allows training and evaluation to be conducted only on samples that have a reasonable expectation (and benefit) to be modeled. After both filtering steps, 4.2 million measurements remain for joining with DSM data.

2) *Digital surface model data*: To extract path profiles from raster data, we first generate a rectangular grid of width W [m] at a 1 m resolution in the projected coordinate system in the UK. Orienting the Tx and Rx locations in the center of the transverse axis, we create an array of $(\lfloor d \rfloor \times W)$ sets of evenly-spaced coordinates (where $\lfloor \cdot \rfloor$ denotes the floor function). We choose W to be an odd integer, allowing the Tx and Rx locations to reside on the closest single pixel each, and enabling the creation of a “direct path” feature consisting of a single line in the center of the path. This feature is described in Section III. The final path profiles are extracted using 2D nearest neighbor interpolation of the original raster data at the generated grid points. This results in a 2D DSM array of shape $(\lfloor d \rfloor \times W)$, where we ensure the orientation between Tx and Rx within the arrays is consistent. We choose W to be 61 m to capture the majority of the first Fresnel zone for these frequencies while having a practical computational load.

Finally, we apply earth curvature correction [10, eq. (7-16)] to the DSM heights relative to the Tx, using a spherical radius of 6364.75 km. The 1D path profiles are then cropped from the direct (center) path of the 2D path profiles, yielding an array of shape $(\lfloor d \rfloor \times 1)$ for each measurement.

III. FEATURE AND ARCHITECTURE SELECTION

We formulate this work as an image problem, where each input feature forms a channel [11] of an image (1D or 2D).

A. Feature Selection

Before computing the feature channels, images are re-sampled to have a constant direct path length of 256 pixels. While the majority of path profiles are down-sampled, some of the shorter links result in up-sampling to 256. Initial experimentation was conducted with training on variably-sized

TABLE I
INPUT FEATURES AND NORMALIZATIONS

Channel	Scaling	Locality
Frequency	Divided by 8000 MHz maximum	Globally
Distance from Tx to each pixel	Divided by maximum link distance in the dataset	Globally
Surface	Normalized (0, 1) using heights of surface and direct path channels	Per sample
Height of direct path from Tx to Rx		

arrays with lengths proportional to the corresponding link distances. This approach yielded poor results, achieving 8-10 dB RMSE with significantly more computational requirements. Re-sampling to a uniform size allows for the design of a single architecture that generalizes well for all link distances.

In the re-sampled arrays, we include the essential features, frequency and distance, as their own channels. Frequency (MHz) is encoded as a channel with a constant value, while the distance channel is generated by computing the 2D Euclidean distance in metres from the Tx to each pixel. The distance channel serves the dual purpose of encoding relative spatial locations [12] while providing the non-sampled distances.

We use two additional channels to capture path profile information: (1) surface and (2) direct path. Surface (DSM) provides the model with the path profile height information and direct path provides the antenna locations, heights and the direct path from Tx to Rx antennas. In the case of the 2D path profiles, the pixels in the center of the transverse dimension contain the direct path heights and are 0 elsewhere in the channel.

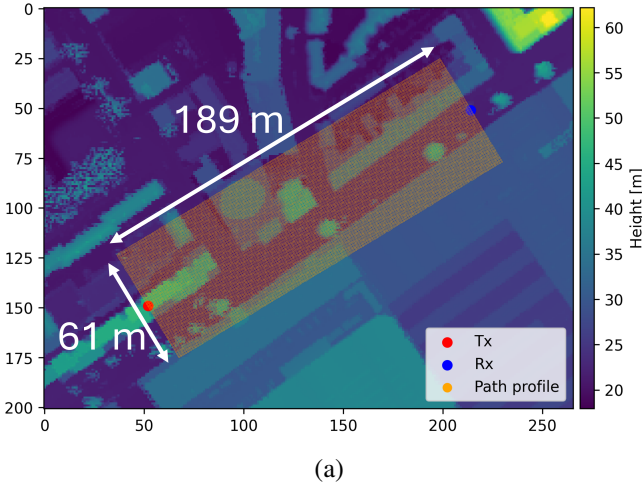
The path profile extraction process and results are shown in Fig. 1 for a link in London with a distance of 189 m. The final dataset contains samples of shape: $(4 \text{ channels} \times 256 \text{ length} \times N \text{ width})$, where N is 1 for the 1D method and 61 for the 2D method.

All features and their normalizations are summarized in Table I. Locality refers to where the normalization is retrieved from. All heights are normalized on a per-sample basis. While the model is able to exploit the frequency dependence of the features in the transverse dimension, we note that normalizing the heights for each sample prevents the model from fully exploiting frequency dependence along the height dimension, by not having access to the scale of the heights. Attempts to include height scaling within the input yielded significant overfitting. Frequency dependence is fully exploitable by the model along the transverse dimension, since this dimension is not re-sampled, and distances and frequencies are both present.

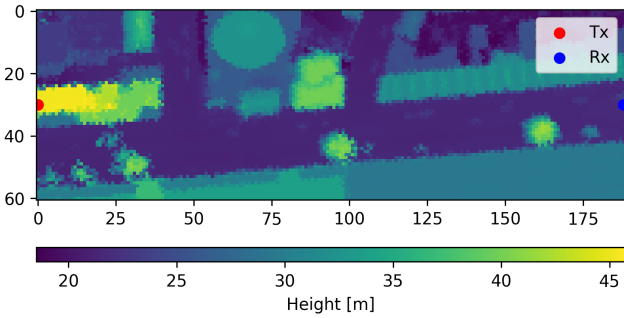
Re-sampled and normalized inputs to the 1D and 2D path loss models are shown in Fig. 2 and Fig. 3 respectively for a 449 MHz link in London.

B. Model Architectures

Given the spatial structure of the data, we employ convolutional neural networks (CNNs) [11], treating the data as images. We design two CNNs: one for processing the 1D path profiles, and another for the 2D path profiles. The 2D CNN is designed identically to the 1D CNN, except all kernels



(a)



(b)

Fig. 1. Path profile extraction process for a link in London. Clutter presents as higher intensity, while roads present as lower intensity. (a) Subset of raster used for path profile extraction. (b) Extracted path profile (not normalized).

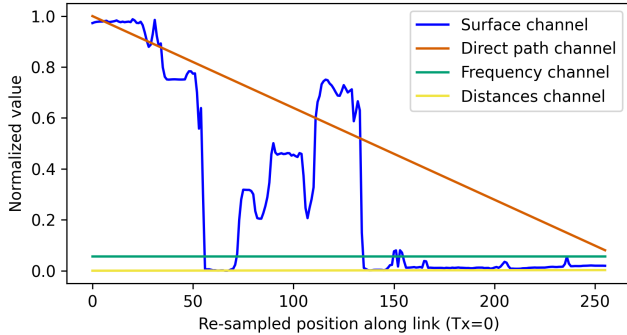


Fig. 2. Re-sampled and normalized four-channel input to 1D CNN.

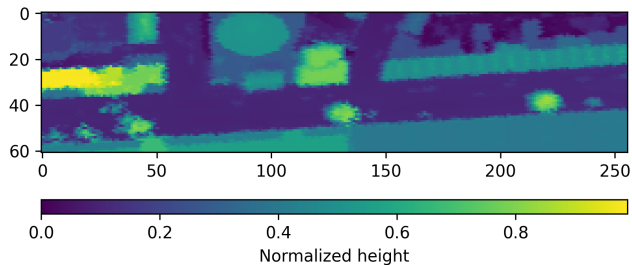


Fig. 3. Re-sampled and normalized surface channel input to 2D CNN.

TABLE II
STRUCTURE OF 1D AND 2D CNNs

Layer	Output image shape (channels \times length \times [1D or 2D width])
Input	$4 \times 256 \times [1 \text{ or } 61]$
Convolution + ReLU	$32 \times 256 \times [1 \text{ or } 61]$
Max pool	$32 \times 128 \times [1 \text{ or } 31]$
Convolution + ReLU	$64 \times 128 \times [1 \text{ or } 31]$
Max pool	$64 \times 64 \times [1 \text{ or } 16]$
Convolution + ReLU	$128 \times 64 \times [1 \text{ or } 16]$
Max pool	$128 \times 32 \times [1 \text{ or } 8]$
Convolution + ReLU	$256 \times 32 \times [1 \text{ or } 8]$
Max pool	$256 \times 16 \times [1 \text{ or } 4]$
Convolution + ReLU	$512 \times 16 \times [1 \text{ or } 4]$
Max pool	$512 \times 8 \times [1 \text{ or } 2]$
Convolution + ReLU	$1024 \times 8 \times [1 \text{ or } 2]$
Max pool	$1024 \times 4 \times 1$
Flatten + Dropout @ 0.25	4096
Fully connected + ReLU	256
Fully connected	1

are square windows of the same size, rather than linear. Each convolution layer has a kernel size of 3, stride size of 2, and zero-padding size of 1. Each max pool layer has a kernel size of 3, stride size of 1, and “same” zero-padding [11].

During training, we use dropout at a rate of 25% on the flattened features to minimize overfitting. The extracted features are input to a fully connected network (FCN) [11] with 256 hidden units and rectified linear unit (ReLU) activation. The final output is path loss.

We design the 2D CNN model identically to the 1D model on the length axis. The transverse axis kernel sizes are chosen such that the image dimensions decrease at the same rate, resulting in the same number of features. Given the low RMSE in [3] with only 3 features, 4096 features are likely to be sufficient, regardless of the feature extraction process.

The network structure is summarized in Table II. The 1D and 2D models have total parameter counts of 3 146 593 and 7 337 569 respectively. Both neural networks are developed, trained, and evaluated in PyTorch [13]. The following section describes the training regimen and evaluation results.

IV. TRAINING AND RESULTS

To decrease training times, a random subset of the filtered data is taken to compare the two models. 10 000 samples are taken from each frequency/city combination, resulting in 60 000 samples per city, for a total of 360 000 samples.

We perform a six-city cross-validation, where each city is separately held out as the test set, with the remaining five cities split between training and validation. We use adaptive moment estimation (Adam) [14] with a learning rate of 0.0001 and batch size of 256 for 200 epochs. The model with the lowest validation RMSE is used to evaluate test RMSE.

A. Validation Split

Deep learning models are more likely to overfit to GIS arrays (feature-rich) than scalar features (feature-sparse) for the same amount of data, given the difference in dimensionality [15]. To mitigate this, for each city holdout, we geographically split each of the remaining five cities using

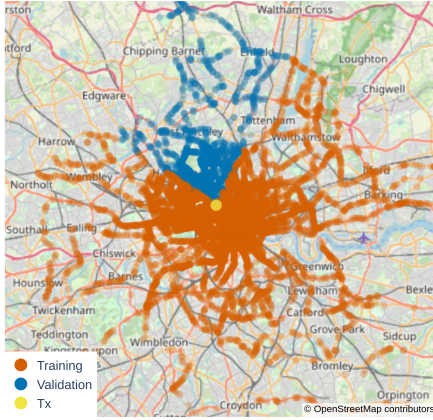


Fig. 4. Example of geographic training-validation split in London.

TABLE III
CROSS-VALIDATION HOLDOUT RMSE (dB) ACROSS 10 RUNS

Holdout	1D CNN		2D CNN		Benchmarks [3]	
	Mean	SD	Mean	SD	P.1812	FCN
Boston	7.78	0.60	7.18	0.27	11.4	7.56
London	9.95	0.89	7.75	0.47	8.8	7.44
Merthyr Tydfil	8.09	0.44	8.07	0.39	13.4	7.22
Nottingham	7.16	0.30	6.99	0.23	12.6	7.07
Southampton	6.62	0.45	6.35	0.42	9.5	6.64
Stevenage	7.65	0.31	7.73	0.21	12.3	8.81
Mean	7.88	0.50	7.35	0.33	11.3	7.46

80% for training and 20% for validation. In each of these five cities, an initial angle θ is chosen. Rotating counter-clockwise about the Tx, the first 20% of Rx locations encountered are used as validation samples, with the remaining 80% used for training. A geographic split for each of the five non-holdout cities provides diverse yet geographically distinct training and validation sets. This split is necessary with this feature set, as initial studies using random splits caused significant overfitting due to high correlation with training sets. Fig. 4 shows an example of a training-validation split in London.

B. Evaluation of Result Consistency

Each city holdout is conducted 10 times with different random seeds to evaluate model robustness. For each training run, we sample a 20% subset (2000 samples) from each city/frequency combination from the original 10 000 subset, for a total of 72 000 samples (48 000 training, 12 000 validation, and 12 000 test). Each run has a random 20% subset, initial weights, training data shuffling, and initial validation angle θ for each city.

Table III summarizes the cross-validation results with a mean and standard deviation (SD) of RMSE for both models. We also compare the mean results with ITU-R P.1812-6 [2] (the industry standard for 1-6 GHz, hereafter referred to as P.1812) and a three-feature FCN using frequency, distance, and total obstruction depth [3].

The 2D models generally have lower RMSE than 1D models, benefiting from the additional transverse information in the 2D path profiles, and resulting in more pertinent features.

Compared to the FCN, our 2D model shows lower mean RMSE on four of six holdouts, with higher mean RMSE on

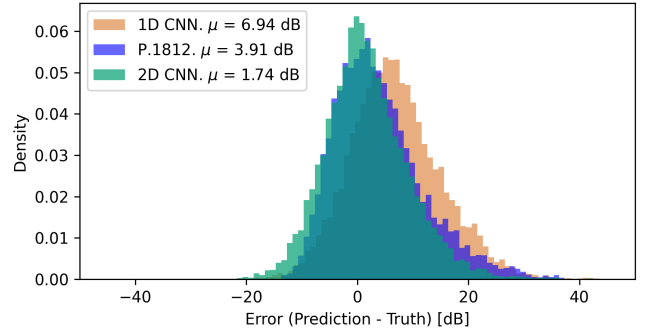


Fig. 5. Histogram of prediction errors for first London holdout.

the other two holdouts (London and Merthyr Tydfil). Our 1D model has higher mean RMSE than the FCN on four of six holdouts. Although some of the holdouts show lower RMSE than the FCN, the fact that other holdouts have higher RMSE in the presence of richer feature sets suggests a further need for model refinement and feature selection.

Generally, our modeling approaches provide significant improvement over the current industry standard. Across all models and holdouts, our CNNs have lower RMSE than P.1812 in 11 of 12 cases, with the only exception being the 1D London-holdout model. This indicates that higher-dimensional information outperforms representative clutter heights for predictive modeling purposes. Fig. 5 shows the error distribution for the CNNs and P.1812 for a single-run London holdout (the lowest drive test RMSE for P.1812). Across runs and holdouts, the 2D model consistently has mean error closest to 0 dB.

Merthyr Tydfil and London are the two holdouts with the highest RMSE. Despite sequential overfitting [16] to the London holdout, the other four cities show strong generalization. Since London contains the highest clutter density among the six cities, and Merthyr Tydfil contains the highest terrain density, it is more challenging to generalize high-dimensional GIS features to these two holdouts. Test performance may be improved by providing the difference between terrain and clutter via a terrain channel.

Future studies will investigate additional feature channels to decrease test RMSE, such as height scaling and Fresnel information within the path profiles, terrain to distinguish between clutter and ground, and type of clutter. Future work may also investigate further validation splitting techniques to minimize overfitting.

V. CONCLUSION

Path loss modeling is an asset for effective radio deployments and spectrum planning. This paper described the use of CNNs in conjunction with surface path profiles to train a path-specific path loss model with low test RMSE in a variety of environments. We showed that CNNs trained on 2D path profiles outperform a modern FCN path loss model with equivalent scalar features in four of six holdouts. We also showed that CNNs trained on both 1D and 2D path profiles consistently achieve lower RMSE than the industry standard in a variety of communications environments, without the need for derived clutter metrics or scalar features.

ACKNOWLEDGMENT

The authors of this paper would like to thank Mathieu Châteauevert from Communications Research Centre Canada (CRC) for his support with propagation and GIS, as well as Alexis Bose (CRC) and Paul Guinand (CRC) for their advice on machine learning strategies.

REFERENCES

- [1] "Prediction of tropospheric radio transmission over irregular terrain, a computer method-1968," in *ESSA Tech. Rep. ERL 79-ITS 67*. U.S. Gov. Printing Office, Washington, DC, July 1968.
- [2] "P.1812: A path-specific propagation prediction method for point-to-area terrestrial services in the frequency range 30 MHz to 6000 MHz," International Telecommunications Union (ITU). [Online]. Available: <https://www.itu.int/rec/R-REC-P.1812-6-202109-1/en>. Accessed August 2024.
- [3] J. Ethier and M. Châteauevert, "Machine learning-based path loss modeling with simplified features," *IEEE Antennas and Wireless Propagation Letters (Early Access)*, pp. 1–5, 2024.
- [4] C. A. Balanis, *Antenna Theory: Analysis and Design*. Wiley and Sons Incorporated, 2005.
- [5] T. Hayashi and K. Ichige, "A deep-learning method for path loss prediction using geospatial information and path profiles," *IEEE Transactions on Antennas and Propagation*, vol. 71, no. 9, pp. 7523–7537, 2023.
- [6] D. R. Roberts *et al.*, "Cross-validation strategies for data with temporal, spatial, hierarchical, or phylogenetic structure," *Ecography*, vol. 40, no. 8, pp. 913–929, 2017. [Online]. Available: <https://nsojournals.onlinelibrary.wiley.com/doi/abs/10.1111/ecog.02881>
- [7] "UK mobile measurement data for frequencies below 6 GHz," Ofcom. [Online]. Available: <https://www.itu.int/md/R15-WP3K-C-0294>. Accessed August 2024.
- [8] Ofcom, "Open data," [Online]. Available: <https://www.ofcom.org.uk/about-ofcom/our-research/opendata>. Accessed November 2024.
- [9] "Open data," Government of the United Kingdom. [Online]. Available: <https://www.data.gov.uk/>. Accessed August 2024.
- [10] D. T. Gillins, M. L. Dennis, and A. Y. Ng, "7.12.9: Point codes," in *Surveying and Geomatics Engineering - Principles, Technologies, and Applications*. American Society of Civil Engineers (ASCE), 2022, p. 227.
- [11] I. Goodfellow, Y. Bengio, and A. Courville, *Deep Learning*. MIT Press, 2016, <http://www.deeplearningbook.org>.
- [12] R. Liu *et al.*, "An intriguing failing of convolutional neural networks and the coordconv solution," 2018. [Online]. Available: <https://arxiv.org/abs/1807.03247>
- [13] A. Paszke *et al.*, "PyTorch: An imperative style, high-performance deep learning library," in *Advances in Neural Information Processing Systems 32*. Curran Associates, Inc., 2019, pp. 8024–8035. [Online]. Available: <http://papers.neurips.cc/paper/9015-pytorch-an-imperative-style-high-performance-deep-learning-library.pdf>
- [14] D. P. Kingma and J. Ba, "Adam: A method for stochastic optimization," in *3rd International Conference on Learning Representations, ICLR 2015*, Y. Bengio and Y. LeCun, Eds., San Diego, CA, USA, May 7-9, 2015. [Online]. Available: <http://arxiv.org/abs/1412.6980>
- [15] U. Braga-Neto, *Fundamentals of Pattern Recognition and Machine Learning*, 2nd ed. Springer International Publishing, 2024.
- [16] M. A. Lones, "Avoiding common machine learning pitfalls," *Patterns*, vol. 5, no. 10, p. 101046, Oct. 2024. [Online]. Available: <http://dx.doi.org/10.1016/j.patter.2024.101046>